Monthly Notices
of the
ROYAL ASTRONOMICAL SOCIETY

MNRAS **468,** 2176–2188 (2017)
Advance Access publication 2017 March 9

doi:10.1093/mnras/stx578

Winds of change: reionization by starburst galaxies

Mahavir Sharma,[1]★ Tom Theuns,[1] Carlos Frenk,[1] Richard G. Bower,[1]
Robert A. Crain,[2] Matthieu Schaller[1] and Joop Schaye[3]

[1]*Institute for Computational Cosmology, Department of Physics, University of Durham, South Road, Durham DH1 3LE, UK*
[2]*Astrophysics Research Institute, Liverpool John Moores University, 146 Brownlow Hill, Liverpool L3 5RF, UK*
[3]*Leiden Observatory, Leiden University, PO Box 9513, NL-2300 RA Leiden, the Netherlands*

Accepted 2017 March 6. Received 2017 March 5; in original form 2016 June 28

ABSTRACT

We investigate the properties of the galaxies that reionized the Universe and the history of cosmic reionization using the 'Evolution and Assembly of Galaxies and their Environments' (EAGLE) cosmological hydrodynamical simulations. We obtain the evolution of the escape fraction of ionizing photons in galaxies assuming that galactic winds create channels through which 20 per cent of photons escape when the local surface density of star formation is greater than 0.1 $\mathrm{M_\odot\ yr^{-1}\ kpc^{-2}}$. Such threshold behaviour for the generation of winds is observed, and the rare local objects that have such high star formation surface densities exhibit high escape fractions of $\sim$10 per cent. In our model, the luminosity-weighted mean escape fraction increases with redshift as $\bar{f}_{\rm esc} = 0.045\,((1+z)/4)^{1.1}$ at $z > 3$, and the galaxy number weighted mean as $\langle f_{\rm esc}\rangle = 2.2\times10^{-3}\,((1+z)/4)^{4}$, and becomes constant $\approx$0.2 at redshift $z > 10$. The escape fraction evolves as an increasingly large fraction of stars forms above the critical surface density of star formation at earlier times. This evolution of the escape fraction, combined with that of the star formation rate density from EAGLE, reproduces the inferred evolution of the filling factor of ionized regions during the reionization epoch ($6 < z < 8$), the evolution of the post-reionization ($0 \leq z < 6$) hydrogen photoionization rate and the optical depth due to Thomson scattering of the cosmic microwave background photons measured by the *Planck* satellite.

Key words: galaxies: evolution – galaxies: formation – galaxies: starburst – cosmology: theory – dark ages, reionization, first stars.

1 INTRODUCTION

The hot Universe emerging from the big bang cooled as it expanded and, at a redshift of $z \sim 1100$, reached a temperature of $T \sim 3000$ K, cold enough for the hydrogen in the primordial gas to become neutral (Mather et al. 1994). By a redshift of $z \sim 100$, the temperature had dropped further so that the radiation temperature corresponded to infrared wavelengths and the Universe became effectively dark. These 'dark ages' came to an end as hot stars in the first galaxies emitted photons with energies greater than the ionization potential of hydrogen, (re)ionizing and heating the gas to a temperature of $T \sim 10^4$ K. Other sources of photons could have played a role as well.[1]

Regions around the first galaxies were ionized first, growing in number and size until they eventually coalesced as more and brighter star-forming galaxies appeared (e.g. Ciardi et al. 2000; Gnedin 2000; Miralda-Escudé, Haehnelt & Rees 2000; Keller et al. 2014; Furlanetto & Oh 2016). Therefore, as reionization proceeded, an increasingly large fraction of the Universe became ionized. The temporal history of reionization can therefore be quantified by the evolution of the volume filling factor of ionized gas as a function of redshift, $Q_{\rm H\,II}(z)$.

Measurements of the column density of electrons between us and the surface of last scattering (the Thomson optical depth; e.g. Planck Collaboration XLVII 2016), the frequency of patches containing neutral gas as measured in quasar spectra ('dark gaps'; McGreer, Mesinger & D'Odorico 2015), the rapid evolution in the number density of galaxies detected in Lyman α (Lyα) emission and their clustering (e.g. Ota et al. 2008; Ouchi et al. 2010; Caruana et al. 2012; Ono et al. 2012; Schenker et al. 2014; Tilvi et al. 2014), the presence of neutral gas around high-redshift quasars (e.g. Mortlock et al. 2011) and gamma-ray bursts (e.g. Totani et al. 2014) are all consistent with a Universe that is mostly neutral ($Q_{\rm H\,II} \sim 0$) at

★ E-mail: mahavir.sharma@durham.ac.uk

[1] For reviews on the science of reionization see e.g. Barkana & Loeb (2001) and Fan, Carilli & Keating (2006); for recent discussions of how this science drives the design of future observatories, see e.g. Stiavelli et al. (2009) for the *James Webb Space Telescope* (*JWST*) and Mellema et al. (2013) and Iliev et al. (2015) for the Square Kilometer Array (SKA).

$z \gtrsim 8$ and highly ionized ($Q_{\rm H\,II} \sim 1$) at $z \lesssim 6$; see Robertson et al. (2015), Bouwens et al. (2015b) and Fig. 8 below. A more quantitative characterization of this ionization phase transition may require detection of the signal of residual neutral hydrogen (H I) with the next generation of radio telescopes.

Once a hydrogen atom has been ionized, it can recombine with a free electron. The equation describing the evolution of $Q_{\rm H\,II}$ therefore contains a term describing photoionization and a term describing recombination (e.g. Haardt & Madau 2012):

$$\dot{Q}_{\rm H\,II} = \frac{\bar{f}_{\rm esc}\dot{n}_{\gamma,\star}}{\langle n_{\rm H}\rangle} - 1.08\,\alpha_{\rm B}\,\mathcal{C}\langle n_{\rm H}\rangle Q_{\rm H\,II}, \quad (1)$$

where $\dot{n}_{\gamma,\star}$ is the rate at which ionizing photons are produced per unit volume [it is proportional to the cosmic star formation rate (SFR) density: $\dot{n}_{\gamma,\star} = f_\star\,\dot{\rho}_\star$, where f_* depends on the properties of the stellar population such as its initial mass function (IMF)]; $\bar{f}_{\rm esc}$ is the mean fraction of ionizing photons that escape from galaxies; $\langle n_{\rm H}\rangle$ is the mean hydrogen number density; $\alpha_{\rm B}$ is the recombination coefficient; the factor 1.08 accounts for the reionization of He I to He II and $\mathcal{C} \equiv \langle n_{\rm H}^2\rangle/\langle n_{\rm H}\rangle^2$ is the clumping factor (e.g. Pawlik, Schaye & van Scherpenzeel 2009) that takes into account absorption by Lyman limit systems (LLSs). A complete radiative transfer calculation is required to estimate rigorously the effect of LLSs and accounting for spatial variations in the ionized filling factor (e.g. Shukla et al. 2016). However, equation (1) is used extensively and provides a reasonable description of the global reionization history (Haardt & Madau 2012; Bouwens et al. 2015b; Madau & Haardt 2015; Mitra, Choudhury & Ferrara 2015; Robertson et al. 2015; Gnedin 2016; Khaire et al. 2016).

After reionization, the Universe is highly ionized with islands of neutral, or almost neutral gas. The distribution of these neutral absorbers sets the mean free path of an ionizing photon, with the higher column density absorbers (neutral column $N_{\rm H\,I} \gtrsim 10^{17}\,{\rm cm}^{-2}$) acting as photon sinks which determine the hydrogen photoionization rate, $\Gamma_{\rm H\,I}$, for a given photon emissivity, $\bar{f}_{\rm esc}\,\dot{n}_\gamma$. Many models of reionization simply tune $\bar{f}_{\rm esc}\dot{n}_\gamma$ to reproduce the observed evolution of $\dot{Q}_{\rm H\,II}$ but a successful model should also reproduce the observed value of $\Gamma_{\rm H\,I}$ at redshifts lower than the redshift of reionization.

The low observed value of the escape fraction in present-day galaxies (e.g. Bland-Hawthorn & Maloney 2001 find at most a few per cent for the Milky Way), and the measured evolution of $\dot{n}_\gamma$, $Q_{\rm H\,II}$ and $\Gamma_{\rm H\,I}$ over the redshift range $z = 3$–8 are inconsistent with $\bar{f}_{\rm esc}$ remaining constant in time. Instead, the escape fraction should increase rapidly with redshift, $\bar{f}_{\rm esc} \approx 1.8 \times 10^{-4}\,(1+z)^{3.4}$, according to Haardt & Madau (2012) (see also Faisst 2016; Gnedin 2016; Khaire et al. 2016; Price, Trac & Cen 2016). Consistent with this, Bolton & Haehnelt (2007) and Pawlik et al. (2009) claim that the escape fraction of galaxies at $z \sim 6$ should be of order 20 per cent to account for the (high) ionization level of the hydrogen gas in the intergalactic medium (IGM). Few, if any, observed values of $f_{\rm esc}$ in galaxies at $z < 3$ are as high as 20 per cent.

Direct evidence that the escape fraction increases with redshift is somewhat inconclusive; claimed detections of ionizing photons leaking from galaxies are controversial (Mostardi et al. 2015). Bridge et al. (2010), Siana et al. (2010) and Rutkowski et al. (2016) detect no ionizing photons escaping at all from galaxies at $z \sim 1$, with 3σ upper limits of the order of 2 per cent. Typically 10 per cent of the $z \sim 3$ Lyman-break galaxies (LBGs) show detectable escaping Lyman continuum photons ($f_{\rm esc} \sim 10$ per cent; Siana et al. 2007, 2010). Iwata et al. (2009) report similar values in a Subaru Deep Field survey, as do Nestor et al. (2013) from *Hubble Space Telescope* (*HST*) data. Vanzella et al. (2012) report a detection $f_{\rm esc} \approx 24$ per cent from a $z = 4$ LBG. Matthee et al. (2017) claim detection of escape fractions as high as 60 per cent from brighter galaxies in their sample at $z \geq 2$. Leitet et al. (2013) claim that observed escape fractions are higher for galaxies with higher specific star formation rates (sSFRs). Observations by Zastrow et al. (2011, 2013) indicate that ionizing photons escape through cones presumably created by galactic winds.

Numerical simulations that include radiative transfer face the formidable challenge of modelling accurately the structure of the absorbing interstellar medium (ISM; e.g. Pawlik, Schaye & Dalla Vecchia 2015; Pawlik et al. 2017) and simulations performed by different groups yield rather contradictory results, ranging from a very low value of a few per cent (e.g. Gnedin, Kravtsov & Chen 2008) to very high values of $f_{\rm esc} = 80$ per cent during starbursts at high redshift (e.g. Wise & Cen 2009; Wise et al. 2014). Furthermore, Wise & Cen (2009) find the escape fraction to increase with increasing halo mass but Razoumov & Sommer-Larsen (2010), Yajima, Choi & Nagamine (2011) and Paardekooper, Khochfar & Dalla Vecchia (2015) find the opposite trend.

What these simulations do have in common is that the feedback from supernovae (SNe) associated with recent star formation generates large density contrasts in the ISM, puncturing channels through which winds and presumably also ionizing photons escape (e.g. Razoumov & Sommer-Larsen 2006; Gnedin et al. 2008; Wise & Cen 2009; Yajima et al. 2011; Ma et al. 2015; Pawlik et al. 2015, 2017; Trainor et al. 2015), a fact that is also indicated by the dependence of escape fraction on sSFR commonly reported in such simulations. Such outflows are observed in $z \sim 3$ LBGs (e.g. Pettini et al. 2002), lower redshift $z \sim 1$ galaxies (e.g. Erb et al. 2012) and in local starbursts (e.g. Strickland & Heckman 2009). Simulations of galaxy formation generate winds and these regulate star formation, with large mass-loading factors in lower mass galaxies ($M_* < 10^{10}\,{\rm M}_\odot$) to avoid overproducing the faint-end of the galaxy luminosity function (e.g. White & Rees 1978; White & Frenk 1991). It is these winds that are thought to enrich the low-density IGM with metals (e.g. Madau, Ferrara & Rees 2001; Theuns et al. 2002; Booth et al. 2012).

Heckman (2001, see also Heckman 2002) used Hα, NaD and X-ray observations to claim that efficient winds are launched provided the surface density of star formation, $\dot{\Sigma}_\star$, exceeds a threshold value of $\dot{\Sigma}_{\star,{\rm crit}} = 0.1\ {\rm M}_\odot\ {\rm yr}^{-1}\ {\rm kpc}^{-2}$, a finding that is also supported by theoretical studies (e.g. Murray, Ménard & Thompson 2011; Scannapieco, Gray & Pan 2012; Scannapieco 2013). If such winds are indeed instrumental in clearing the path for the escape of ionizing photons, then we would expect galaxies with strong winds to have high(er) escape fractions (Heckman et al. 2011) – at least in the absence of absorption by dust, likely a good approximation at the high redshifts ($z > 6$) of the reionization era. The few detections of large escape fractions do indeed correspond to galaxies undergoing an intense starburst with high SFRs, $\dot{M}_\star \gtrsim 10\ {\rm M}_\odot\ {\rm yr}^{-1}$ occurring in a compact region (area $S \approx (1\,{\rm kpc})^2$), hence $\dot{M}_\star/S \gg 0.1\ {\rm M}_\odot\ {\rm yr}^{-1}\ {\rm kpc}^{-2}$ (Borthakur et al. 2014; de Barros et al. 2016; Izotov et al. 2016a,b). Heckman's model would suggest that these galaxies should drive outflows. This is the case for galaxy J0921+4509 discussed by Borthakur et al. (2014) which indeed drives a strong wind (Heckman et al. 2011); it would be very interesting to verify this feature in other galaxies with large $f_{\rm esc}$.

Existing work has not yet integrated these ideas into models of reionization. Instead, analytic or semi-analytic studies generally assume a constant value of $f_{\rm esc}$ for all galaxies at a given redshift

(e.g. Bouwens et al. 2015b; Robertson et al. 2015). We have developed a formalism, described in Sections 3 and 4, in which the escape fraction of ionizing photons from a galaxy is closely intertwined with its feedback activity and therefore varies from galaxy to galaxy. We first outlined and applied this formalism in Sharma et al. (2016) to identify the galaxies that contribute the most to the ionizing radiation and found that the brighter galaxies at high redshift, which are above the *HST* detection limit, provide a large fraction (≈50 per cent) of the ionizing photons responsible for reionization.

In this paper, we investigate the history of reionization analysing galaxies from the 'Evolution and Assembly of Galaxies and their Environments' (EAGLE) suite of cosmological hydrodynamical simulations (Crain et al. 2015; Schaye et al. 2015). We infer the evolution of the escape fraction, and this enables us to calculate the evolution of the filling factor of ionized gas and the electron scattering optical depth and, crucially, verify that we obtain a realistic evolution for the post-reionization amplitude of the ultraviolet (UV) background. The results are particularly interesting in the aftermath of the recently revised lower values of the optical depth by Planck Collaboration XLVII (2016), implying that the Universe was reionized rather later than previously thought (e.g. Haardt & Madau 2012).

This paper is organized as follows. In Section 2, we describe the implementation of subgrid physics in the EAGLE simulation, particularly the aspects that are relevant to this paper. In Section 3, we compare the star formation history from EAGLE to the observations, and study the evolution of the SFR and related quantities. We then explore the properties of the star-forming regions within galaxies, and derive the escape fraction of ionizing photons in Section 4. In Section 5, we compute the ionizing emissivity, the photoionization rate and the electron scattering optical depth. We compare our results with observations and discuss our findings in the final section.

2 THE EAGLE SIMULATIONS

In this work we use the EAGLE suite of cosmological hydrodynamical simulations (Crain et al. 2015; Schaye et al. 2015). These were performed with the GADGET-3 implementation (last described by Springel 2005) of the tree-smoothed particle hydrodynamics (SPH) algorithm, with 'subgrid' modules for physical processes below the resolution limit. We briefly review these modules here, paying particular attention to the star formation and reionization implementations, since these are the most relevant to this paper.

The simulations are performed in cubic periodic volumes and start redshift of 127 from cosmological initial conditions generated using second-order Lagrangian perturbation theory, as described by Jenkins (2013). We use the Planck Collaboration XVI (2014) values of the cosmological parameters. The simulation takes advantage of improvements to the basic SPH and time stepping algorithms implemented in GADGET-3, which we collectively refer as ANARCHY. These are described by Schaye et al. (2015), with Schaller et al. (2015) illustrating their relatively small effects on the properties of galaxies. The simulation tracks 11 elements (H, He, C, N, O, Ne, Mg, Si, S, Ca and Fe) released during the evolution of massive stars, asymptotic giant branch (AGB) stars and Type I and Type II SNe, as described in Wiersma et al. (2009b).

Element-by-element cooling and photoheating by the optically thin UV/X-ray background of Haardt & Madau (2001), including Compton cooling and thermal bremsstrahlung, are implemented as described by Wiersma, Schaye & Smith (2009a). We assume here that hydrogen reionizes at redshift[2] $z = 11.5$, when we inject an extra 2 eV of energy per hydrogen atom to take into account of non-equilibrium effects that occur when neutral gas is overrun by an ionization front (Abel & Haehnelt 1999). At higher z we impose a uniform radiation field but ignore photons above 1 Rydberg; this prevents the formation of molecules that are neither tracked nor resolved but would affect the cooling rate.

Star formation is implemented by stochastically converting gas particles into collisionless star particles, at a rate set by the local gas pressure (Schaye & Dalla Vecchia 2008). This reproduces the observed $z = 0$ Kennicutt–Schmidt relation (Kennicutt 1998), and we assume that this relation does not evolve. The SFR is assumed to be zero below the metallicity-dependent threshold of Schaye (2004) for the formation of a cold ($T \ll 10^4$ K) gas phase. Feedback from star formation is implemented thermally as described by Dalla Vecchia & Schaye (2012). The simulation also models the formation, growth and feedback from supermassive black holes, as described by Springel, Di Matteo & Hernquist (2005) and Booth & Schaye (2009), but taking into account the angular momentum of accreting gas, as described by Rosas-Guevara et al. (2015).

The free parameters of the subgrid modules are calibrated using the observed $z \approx 0.1$ galaxy stellar mass function, galaxy sizes and the relation between black hole mass and stellar mass, as described by Crain et al. (2015). EAGLE reproduces a wide range of observables that were not part of the calibration process. Most relevant to this work are the papers by Furlong et al. (2015, 2017) that show EAGLE broadly reproduces the evolution of galaxy masses and sizes, respectively.

In this paper we use three simulations from the EAGLE suite that differ in volume to verify that our results are converged, L0025N0376, L0050N0752 and L0100N1504 in table 2 in Schaye et al. (2015). These adopt identical subgrid models and parameters and are performed in volumes of 25, 50 and 100 comoving megaparsecs on a side, respectively. Gas particles in simulations L025N0376 and L0100N1504 have initial particle masses of $m_g = 1.81 \times 10^6$ M$_\odot$. The comoving Plummer equivalent gravitational softening length is $\epsilon_{com} = 2.66$ kpc and the maximum physical gravitational softening length is $\epsilon_{prop} = 0.70$ kpc. In the higher resolution simulation, L0050N0752, $m_g = 2.26 \times 10^5$ M$_\odot$, $\epsilon_{com} = 1.33$ kpc and $\epsilon_{prop} = 0.35$ kpc.

3 THE EVOLUTION OF THE STAR FORMATION SURFACE DENSITY IN GALAXIES

In this section we demonstrate that the surface density of star formation averaged on kiloparsec scales, $\dot{\Sigma}_\star$, increases rapidly with redshift in EAGLE, examine whether there is observational support for this trend and investigate the underlying physical processes that drive the evolution in the simulation.

The SFR of star-forming galaxies as a function of halo mass,[3] M_h, and the baryon fraction, $f_{baryon} \equiv (M_* + M_{gas})/M_h$, of EAGLE galaxies are plotted at several redshifts in Fig. 1. At $z = 0$, f_{baryon} increases

[2] The epoch of reionization imposed on the simulation is therefore not consistent with what we estimate is the actual epoch of reionization. We verified that this does not impact our conclusions significantly: in these simulations, the effects of reionization on the cosmic SFR are relatively small.

[3] By halo mass, we mean the mass enclosed by a sphere, within which the mean density is 200 times the critical density.

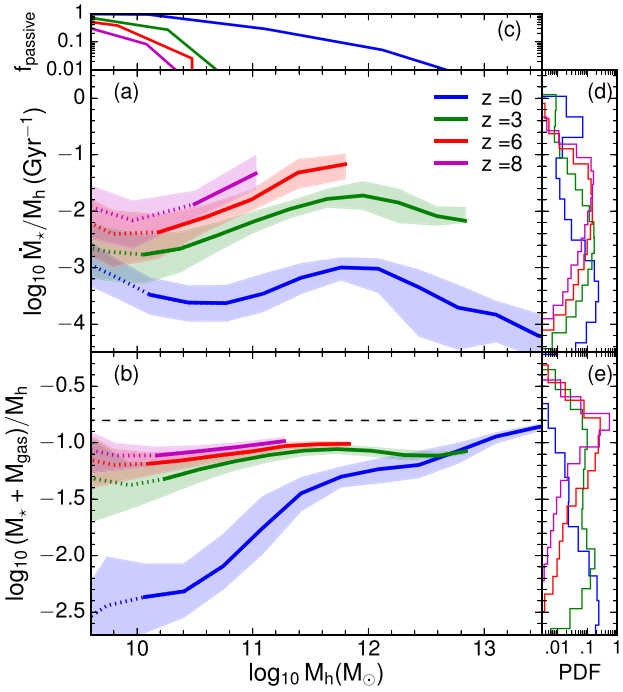

Figure 1. The median SFR ($\dot{M}_\star$; panel a) and the halo baryon fraction (panel b) as a function of the halo mass (M_h) for galaxies in the EAGLE simulation, shown as solid curves for redshift 0 (blue), 3 (green), 6 (red) and 8 (magenta). Shaded regions show the range of 25th–75th percentile. The corresponding passive fractions are shown in panel (c). The probability distribution of $\dot{M}_\star/M_\mathrm{h}$ is plotted in panel (d) and that of the baryon fraction in panel (e). The halo baryon fraction and SFR both increase rapidly with redshift.

strongly with M_h up to $M_\mathrm{h} \approx 10^{12}\,\mathrm{M}_\odot$, and continues to increase above that but at a slower rate. The corresponding SFR $\dot{M}_\star/M_\mathrm{h}$ remains approximately constant up to $M_\mathrm{h} = 10^{12}\,\mathrm{M}_\odot$ and declines at higher M_h. Clearly, $\dot{M}_\star/M_\mathrm{h}$ and f_baryon do not track each other well because star formation is self-regulating with the dense gas fraction set by the efficiency of feedback, as demonstrated by Haas et al. (2013) for galaxies and by Altay et al. (2013) for damped Lyα systems in the OWLS simulations presented by Schaye et al. (2010). In particular, the decline in $\dot{M}_\star/M_\mathrm{h}$ above $M_\mathrm{h} = 10^{12}\,\mathrm{M}_\odot$ is due to active galactic nuclei (AGN) feedback in EAGLE. The feedback in EAGLE is calibrated to reproduce the $z = 0$ stellar mass function and the sizes of galaxies. The simulation then also reproduces the SFR as a function of M_*, with star-forming galaxies having the right colours and with approximately the right fraction of passive red galaxies (Trayford et al. 2015, 2016). Even though EAGLE reproduces well the observed increase in sSFR, $\dot{M}_\star/M_\star$, with z, the values of the sSFR as a function of M_* are typically too low by a factor of 2, as is the SFR density (Furlong et al. 2015, their figs 4 and 5). Furlong et al. (2015) show that, nevertheless, EAGLE reproduces the observationally inferred stellar mass functions well. This may appear contradictory, as the integral of the SFR gives the stellar mass. Mitchell et al. (2013) examined the origin of this apparent discrepancy in the semi-analytical GALFORM model, concluding that several observational biases may play a role.

Towards higher z both f_baryon and $\dot{M}_\star/M_\mathrm{h}$ increase rapidly in EAGLE, while the passive fraction decreases. This leads to the blue cloud of star-forming galaxies becoming bluer with increasing z, and the red sequence thinning out, as shown by Trayford et al. (2016) up to $z = 2$. This trend continues to higher z, with for example the SFR of a galaxy hosted by a halo of mass $M_\mathrm{h} = 10^{11}\,\mathrm{M}_\odot$ increasing by nearly two orders of magnitude from $z = 0$ to 6. These higher SFRs with increasing z result in a luminosity function of EAGLE galaxies that is in good agreement with observations out to $z = 7$, as shown by Furlong et al. (2015), and potentially even higher z, as shown in Fig. 2.

The strong evolution of the SFR at a fixed halo mass is a consequence of a balance between the much higher rate of cosmological accretion at higher z, and the evolution of the efficiency of feedback from star formation (and black holes at higher M_h). In particular, feedback needs to be *more* efficient at higher z to avoid producing too many stars early on. Conversely, we find that feedback needs to be relatively inefficient at low z, because otherwise the sSFR would be lower than observed. In EAGLE these trends emerge through the dependence of the subgrid feedback efficiency on the local gas density and metallicity; see Crain et al. (2015) for an in-depth discussion.

While the sSFRs of galaxies increase with z, their sizes decrease (Fig. 2): for a galaxy with $10^9 < M_*/\mathrm{M}_\odot < 10^{10}$, the sSFR $\dot{M}_\star/M_\star$ increases by two orders of magnitude from $z = 0$ to 8, while its stellar half-mass radius $r_{\star,\,50}$ *decreases* by a factor of $\approx$5 following approximately the scaling $r_{\star,\,50} \propto H(z)^{-2/3}$, where $H(z)$ is the Hubble constant. The evolutionary trends in $\dot{M}_\star/M_\star(z)$ and for $r_{\star,\,50}(z)$, seen in the simulation, are observed as well. Kawamata et al. (2015) infer half-mass radii of $\approx$kiloparsec size for bright $z = 6$–8 galaxies, somewhat smaller than those of the more massive EAGLE galaxies, with a slightly steeper redshift dependence of $\propto(1+z)^{-1.24\pm0.1}$ over the redshift range $z = 2.5$–12.

With the SFR in galaxies increasing with z and their sizes decreasing, the surface density of star formation, $\dot{\Sigma}_\star$, increases rapidly, by two orders of magnitude for a galaxy with $\dot{M}_\star \sim 10\,\mathrm{M}_\odot\ \mathrm{yr}^{-1}$ between $z = 0$ and 6 (Fig. 2). If a high value of $\dot{\Sigma}_\star$ is required to drive strong winds, then we would expect that the fraction of galaxies that drive winds increase rapidly with z. Observations of LBGs indeed show that strong outflows are ubiquitous at high redshift (e.g. Pettini et al. 2001; Shapley et al. 2003; Weiner et al. 2009).

What drives this evolution to higher $\dot{\Sigma}_\star$ at higher z in EAGLE? The SFR volume density, $\dot{\rho}_\star$, and surface density, $\dot{\Sigma}_\star$, are computed using the model of Schaye & Dalla Vecchia (2008):[4]

$$\dot{\rho}_\star \propto p^{(2+\gamma\,(n-1))/(2\gamma)} \approx p^{0.95} \approx \rho^{1.27}, \tag{2}$$

$$\dot{\Sigma}_\star = 0.1\,\mathrm{M}_\odot\ \mathrm{yr}^{-1}\ \mathrm{kpc}^{-2} \left(\frac{p/k_\mathrm{B}}{1.35\times10^5\ \mathrm{K\,cm}^{-3}}\right)^{0.7}, \tag{3}$$

where the gas pressure, p, is related to the gas density by the relation, $p \propto \rho^\gamma$, and k_B is Boltzmann's constant. The proportionality constants in equation (2) and the exponent n are derived from the Kennicutt–Schmidt law (Kennicutt 1998) scaled according to the Chabrier IMF used in EAGLE. In EAGLE we adopt $\gamma = 4/3$ and $n = 1.4$, which yields the numerical values above. The evolution of $\dot{M}_\star$ is then a consequence of the higher values of the pressure at which stars form, increasing by more than two orders of magnitude between $z = 0$ and 6, as shown in Fig. 3. The corresponding increase in $\dot{\Sigma}_\star$ is a factor of 25. A second sequence of higher pressure appears at redshifts $z < 3$ that is due to the effect of metal cooling (see Crain et al. 2015 for further details).

[4] The proportionality constant of equation (3) used in Sharma et al. (2016) is $\pi^{1/2}$ larger, because we used a different expression for the Jeans length in that paper. We verified that the lower value used here does not change any of the results of Sharma et al. (2016).

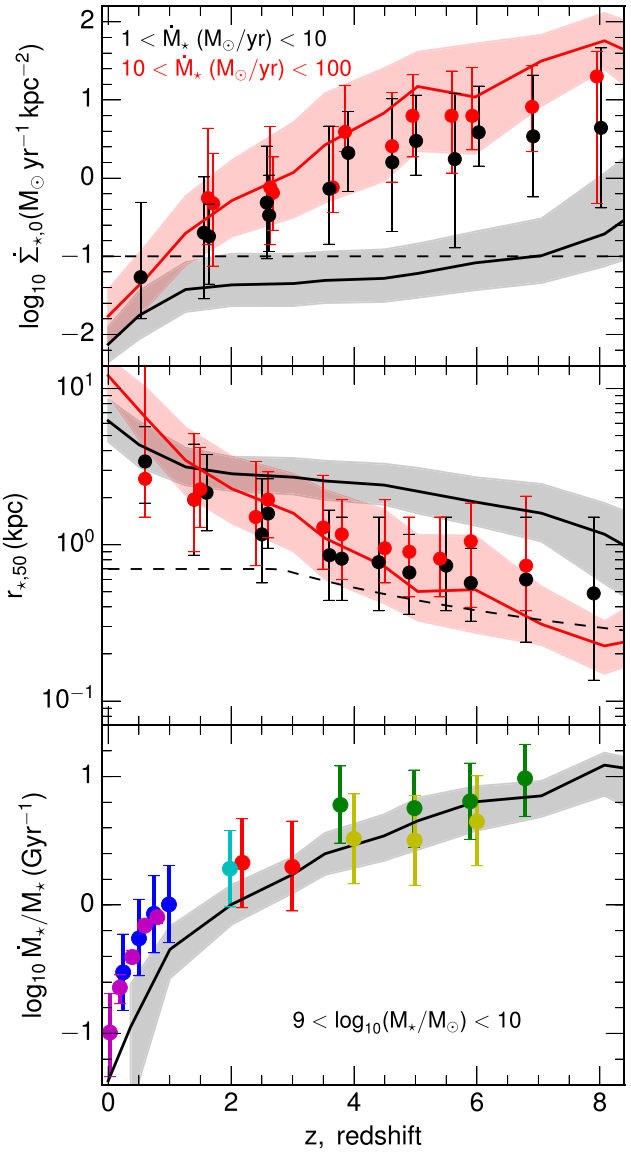

Figure 2. Evolution of the central SFR surface density, $\dot{\Sigma}_{\star,0}$ (top panel), and of the stellar half-mass radius, $r_{\star,50}$ (middle panel), for EAGLE galaxies with SFR $1 < \dot{M}_\star/\mathrm{M}_\odot\ \mathrm{yr}^{-1} < 10$ (black) and $10 < \dot{M}_\star/\mathrm{M}_\odot\ \mathrm{yr}^{-1} < 100$ (red); solid lines show the median relation with the shaded area including the 25th–75th percentiles. Symbols with 1σ error bars are observations from Shibuya, Ouchi & Harikane (2015), with colours corresponding to the same limits in $\dot{M}_\star$. The horizontal dashed line in the top panel denotes the threshold for driving outflows (Heckman 2001) and the dashed line in the middle panel shows the gravitational softening length. There is general agreement between EAGLE and the measurements in that $\dot{\Sigma}_{\star,0}$ increases rapidly with z, although EAGLE galaxies with lower SFR tend to be larger and have lower values of $\dot{\Sigma}_{\star,0}$ than observed at $z > 2$. The bottom panel compares the evolution of $\dot{M}_\star/M_\star$ for EAGLE galaxies with $10^9 < M_*/\mathrm{M}_\odot < 10^{10}$ (black line: median relation, shaded area 25th–75th percentiles) with observational data from Noeske et al. (2007, blue), Damen et al. (2009, magenta), Reddy & Steidel (2009, red), Stark et al. (2013, green), González et al. (2014, orange) and Daddi et al. (2007, cyan). The sSFR in EAGLE increases rapidly with z, tracking the observations, but is low by a factor of ∼0.2–0.3 dex below $z = 1$.

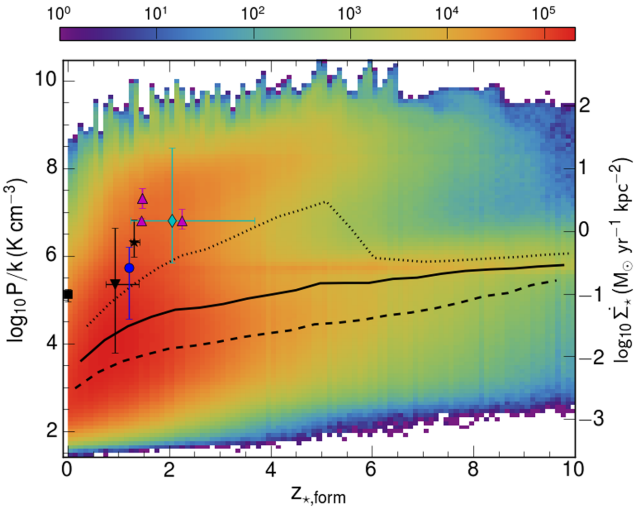

Figure 3. Probability distribution of the pressure at which stars form as a function of redshift. The colour coding is a measure of the fraction of stars that form at a given z with a given pressure; the black solid curve shows the evolution of the median of the birth pressure. The axis on the right shows the corresponding values of $\dot{\Sigma}_\star$ for the star particles from equation (3). The observations with error bars are shown as black square (Kennicutt et al. 2003), blue circle (Freundlich et al. 2013) and magenta triangles (Swinbank et al. 2012). The median birth pressure increases by more than two orders of magnitude between $z \approx 0$ and ≈6, but a small fraction of stars continues to form at high pressure even at $z = 0$. A second sequence of higher birth pressures appears below $z \approx 3$ due to the effects of metal cooling.

The increase in the pressure (or equivalently density since $\rho \propto p^{3/4}$ for star-forming gas in EAGLE) at which stars form is not unique to the EAGLE simulation. We find that in EAGLE the median ISM density at which stars form increases by approximately a factor of 10 between $z = 0$ and 3 (corresponding to an increase in p by a factor of 6); Shirazi, Brinchmann & Rahmati (2014) find an increase by a factor of $7^{+10.2}_{-5.4}$ in electron density in the ISM of galaxies in their sample between redshift 0 and 3, in reasonable agreement with our results.

The observations by Genzel et al. (2011) and Swinbank et al. (2012) of star-forming clumps in highly star-forming galaxies at $z = 1$–2 yield values of $\dot{\Sigma}_\star = 1$–$100\,\mathrm{M}_\odot\ \mathrm{yr}^{-1}\ \mathrm{kpc}^{-2}$, similar again to what we find in EAGLE. These clumps drive strong outflows, which, according to Genzel et al. (2011), are driven by energy injection from massive stars and SNe. This good agreement between EAGLE and these observations confirms that the phenomenology of the physics assumed in the simulations yields realistic results, and gives us confidence that we can reasonably use the results of the simulations to even higher redshifts where the observations are not that constraining.

We conclude that in the EAGLE simulation stars form at increasingly higher gas pressure with increasing z and, as a consequence, the surface density of star formation also increases rapidly. This results in higher z galaxies having higher sSFRs and smaller sizes. These trends quantitatively reproduce observations. In real galaxies (and also in the simulation), such regions of intense star formation drive strong winds and, in the few cases where a measurement of the escape fraction has been possible (Borthakur et al. 2014; de Barros et al. 2016; Izotov et al. 2016a), give rise to relatively high escape fractions, 10–20 per cent. It then follows that the escape fraction of ionizing photons will tend to increase with redshift, as an increasing

fraction of stars is born in galaxies that drive strong outflows. We examine the corresponding evolution of the escape fraction in the next section.

4 THE ESCAPE FRACTION OF IONIZING PHOTONS FROM GALAXIES

Massive stars emit ionizing photons. These can be prevented from escaping their galaxy by absorption by dust, or by being converted to lower energies after first ionizing neutral hydrogen in the galaxy. Their escape fraction, $f_{\rm esc}$, is given by the ratio, $\dot{N}_{\gamma,\rm gal}/\dot{N}_{\gamma,\star}$ of ionizing photons emitted by the *galaxy*, $\dot{N}_{\gamma,\rm gal}$, over that emitted by its *stars*, $\dot{N}_{\gamma,\star}$. Evaluating $f_{\rm esc}$ requires defining where the galaxy 'ends'. Operationally we may take this to mean that the photon escapes out to at least the virial radius, R_{200}, of the galaxy's dark matter halo. Given the two types of photon sinks (dust and H I), we write $f_{\rm esc} = f_{\rm esc,dust} \times f_{\rm esc,H\,I}$, but, since we are mostly interested in the $z > 6$ Universe, we take $f_{\rm esc,\,dust} = 1$ (see e.g. Bouwens et al. 2015b).

The physical reasoning that underlies our model is that strong winds driven by massive stars carve channels through the surrounding (mostly neutral) gas through which ionizing photons can escape. There is some evidence in very high resolution simulations that winds can indeed result in high values of $f_{\rm esc}$, especially if star formation is bursty (e.g. Wise & Cen 2009; Ma et al. 2015), although there is currently no consensus on how, or even if, $f_{\rm esc}$ depends on stellar mass, SFR or redshift (compare, e.g., Kimm & Cen 2014 with Paardekooper et al. 2015 or Xu et al. 2016).

Theoretically, energy injection by SNe creates a thermalized hot cavity that lies at the centre of an expanding bubble. Following Chevalier & Gardner (1974) we find that $\dot{\Sigma}_\star > 10^{-1.5}\,{\rm M}_\odot\,{\rm yr}^{-1}\,{\rm kpc}^{-2}$ is required to achieve a filling factor close to 100 per cent for the hot media. Clarke & Oey (2002) also find such a threshold behaviour for the percolation of SN-blown bubbles in star-forming discs. Similar limits have been inferred from the simulations of Fujita et al. (2003), von Glasow et al. (2013) and Scannapieco et al. (2012). A threshold is also a requirement for blowing radiatively driven winds from massive star clusters (Murray et al. 2011) which may also play a role in evacuating high-density gas from the surroundings of the sources of ionizing photons, leading to higher escape fractions.

We will therefore assume that the value of $f_{\rm esc}$ for individual star-forming patches in a galaxy depends on the local surface density of star formation, $\dot{\Sigma}_\star$ (averaged on scales of $\approx$1 kpc). As in Sharma et al. (2016), we assume the escape fraction to be zero when $\dot{\Sigma}_\star < \dot{\Sigma}_{\star,\rm crit}$, and $f_{\rm esc} = f_{\rm esc,\,max}$ when $\dot{\Sigma}_\star \geq \dot{\Sigma}_{\star,\rm crit}$. We set $\dot{\Sigma}_{\star,\rm crit} = 0.1\,{\rm M}_\odot\,{\rm yr}^{-1}\,{\rm kpc}^{-2}$, the critical surface density above which star-forming regions are observed to drive strong winds according to Heckman (2001), and use a default value $f_{\rm esc,\,max} = 20$ per cent, motivated by the escape fractions observed in $z \sim 0$ starbursts by Borthakur et al. (2014) and Izotov et al. (2016a). The values of $\dot{\Sigma}_{\star,\rm crit}$ and $f_{\rm esc,\,max}$ are the main parameters in our model, we illustrate how our results change if we vary them below.

Some recent studies point out that there may be a timing mismatch between the maximum of the ionizing emissivity and the peak of the escape fraction. Kimm & Cen (2014) make the point that it will take some time for massive stars to carve channels (see also Ma et al. 2016), and so the escape fraction may increase from very low values when the stars form, to high values later on. However, since ionizing photons are produced throughout the life of the massive star, and the channels through which photons escape take some time to open, only a small fraction of all photons produced may effectively escape – even if the *escape fraction* eventually reaches high values. However, this problem may not arise for multiple bursts occurring in the same region (e.g. Gentry et al. 2017). Moreover, Stanway, Eldridge & Becker (2016) argue that stellar population synthesis models that include binary stars may play an important role, because these binary stars have high luminosities in ionizing photons even at a time of order 100 Myr after the starburst (and after the massive stars have been able to open up channels through which photons can escape; see also Ma et al. 2016). Binary stars may therefore play an important role in setting the net emissivity of a star-bursting galaxy.

We implement the model for the escape of photons from EAGLE galaxies through winds as follows. We begin by identifying young star particles (age < 100 Myr), and calculate the surface density of star formation at the time they formed, $\dot{\Sigma}_\star$, from their birth density (using equation 3 and the pressure–density relation, $p \propto \rho^{4/3}$, imposed on star-forming gas in EAGLE), which is recorded for every star particle formed. If $\dot{\Sigma}_\star < \dot{\Sigma}_{\star,\rm crit}$ we set $f_{\rm esc} = 0$ for this star-forming region, and if $\dot{\Sigma}_\star \geq \dot{\Sigma}_{\star,\rm crit}$ we set $f_{\rm esc} = f_{\rm esc,\,max} = 20$ per cent. Weighting each star particle by its SFR at birth, we calculate the ionizing luminosity-weighted value of the escape fraction, as well as the ionizing emissivity, for all EAGLE galaxies.

Fig. 4 is a scatter plot of stellar mass, M_*, versus SFR, $\dot{M}_\star$, for EAGLE galaxies (points) at various redshifts, colour coded according to the instantaneous value of $f_{\rm esc}$. As expected, more massive galaxies appear at lower redshift. The left- and right-hand columns allow us to investigate the impact of resolution and simulation volume, since Recal-L025N0752 (right-hand column) has eight times better mass resolution, but 64 times smaller volume than Ref-L100N1504. In both simulations, star formation is very bursty, with galaxies exhibiting a large scatter in $\dot{M}_\star$ at given M_*.

For any value of M_*, the escape fraction is highest for the most star-forming galaxies of that mass. Since such bursty galaxies are rare, they are less well sampled in Recal-L025N0752, as are the more massive galaxies. The top panels show the cumulative contribution to the total emissivity, $f(M < M_*)$, at three redshifts: 50 per cent of the ionizing emissivity comes from galaxies of mass $M_* \lesssim 5 \times 10^6$, 10^8 and $10^{10}\,{\rm M}_\odot$ at redshifts $z = 8$, 6 and 3, respectively (with comparable values of 10^6, 10^8 and $5 \times 10^9\,{\rm M}_\odot$ in Recal-L025N0752).

Therefore, although the stellar masses of the galaxies that produce the bulk of the ionizing photons may be relatively low, their SFRs (and hence their luminosities, since at these high-redshifts galaxies are typically detected at UV rest wavelengths only) are not. At $z = 8$, 50 per cent of the total ionizing emissivity comes from galaxies with $M_* \lesssim 10^{6.5}\,{\rm M}_\odot$, but these have $\dot{M}_\star \sim 10^{-1}\,{\rm M}_\odot\,{\rm yr}^{-1}$ and hence $M_{1500} \sim -16.5$, only just below the current *HST* detection limit (Sharma et al. 2016). At lower z, brighter galaxies dominate the emissivity even more.

In Fig. 5 we plot the escape fraction as a function of the central surface density of star formation of a galaxy, $\dot{\Sigma}_{\star,0} \equiv \dot{M}_\star/(2\pi R_\star^2)$, where R_* is the stellar half-mass radius and $\dot{M}_\star$ the SFR of the galaxy. For a disc in which $\dot{\Sigma}_\star$ falls exponentially with radius, $\dot{\Sigma}_{\star,0}$ is approximately the central value of the surface density of star formation. The escape fraction in the simulations is well described by $f_{\rm esc} = 0.2/(1 + \dot{\Sigma}_{\star,\rm crit}/\dot{\Sigma}_{\star,0})$, shown as a black dashed curve. There is, however, a large amount of scatter at lower redshifts.

Using this model, the escape fraction of EAGLE galaxies is low or zero at low values of $\dot{\Sigma}_{\star,0} \ll \dot{\Sigma}_{\star,\rm crit}$, close to the maximum of 20 per cent allowed by the model at high $\dot{\Sigma}_{\star,0} \gg \dot{\Sigma}_{\star,\rm crit}$, and exhibits a large scatter at intermediate values of $\dot{\Sigma}_{\star,0}$. At $z = 0$, however, a few rare examples do reach the high values close to the maximum

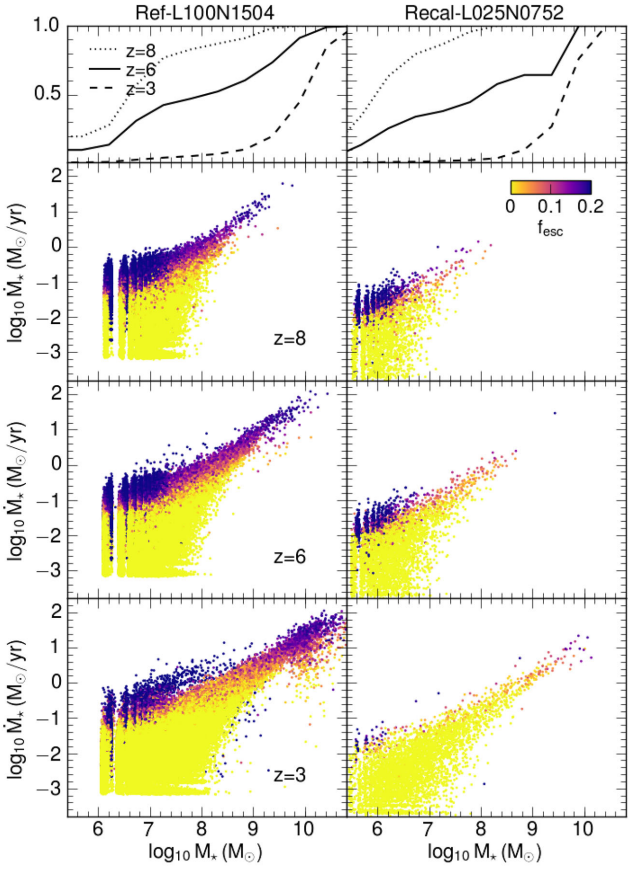

Figure 4. The escape fraction of ionizing photons is shown as a function of the stellar mass (M_*) and the SFR ($\dot{M}_\star$) of the galaxies in the simulation Ref-L100N1504 (left-hand column) and Recal-L025N0752 (right-hand column). In the top row of plots, we show the cumulative number of photons emitted by the galaxies below a given stellar mass, at redshift 3 (dashed), 6 (solid) and 8 (dotted). There is a large amount of scatter in $\dot{M}_\star$ at low M_*, which implies that low mass does not necessarily mean faint. At a given stellar mass, the galaxies with higher SFR (i.e. brighter) have higher escape fractions. the top panel shows that the brighter high-mass galaxies at a given redshift dominate the emissivity. However, the contribution from low-mass galaxies increases with redshift, and at $z = 8$, approximately 50 per cent of the ionizing photons are emitted by galaxies below a stellar mass of 10^7 M$_\odot$. Most of the photons emitted by these low-mass galaxies arise from the brightest ones.

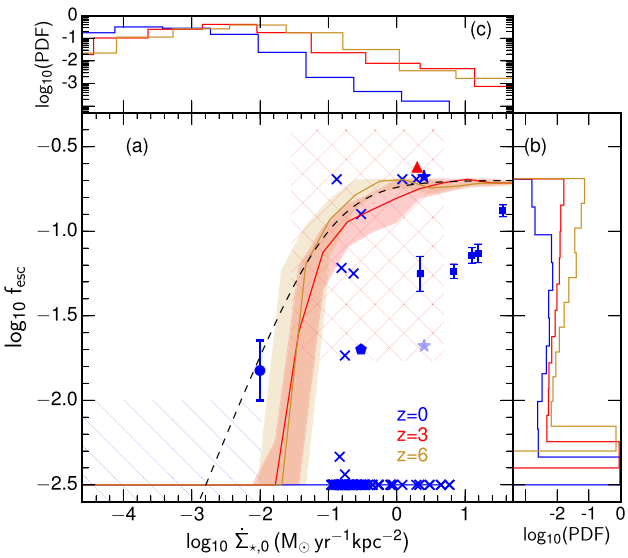

Figure 5. The galaxy-averaged escape fraction of ionizing photons, f_{esc}, as a function of the central surface density of star formation, $\dot{\Sigma}_{\star,0}$, at redshifts $z = 0$ (blue), 3 (red) and 6 (orange), for galaxies with $M_* > 10^7$ M$_\odot$. The galaxies for which $f_{esc} = 0$ have been assigned arbitrarily a value of $\log_{10} f_{esc} = -2.5$. The solid lines correspond to the median escape fractions at each redshift, with the shaded region including the 25th and 75th percentiles; the black dashed line is a simple fit to trend, and is used in the text. The galaxies at $z = 0$ that have $\dot{\Sigma}_{\star,0} > 0.1$ M$_\odot$ yr^{-1} kpc^{-2} are shown as blue crosses. f_{esc} for galaxies with $\dot{\Sigma}_{\star,0} < 10^{-2.5}$ M$_\odot$ yr^{-1} kpc^{-2} is typically very low or zero. For those with $\dot{\Sigma}_{\star,0} > 10^{-1}$ M$_\odot$ yr^{-1} kpc^{-2}, it is typically close to the maximum of 20 per cent allowed by the model, whereas at intermediate values of $\dot{\Sigma}_{\star,0}$ the scatter in f_{esc} is large. The red cross-hashed region represents the observed range of $z \approx 3$ LBGs with confirmed detections of ionizing radiation (Shapley et al. 2006; Iwata et al. 2009; Nestor et al. 2013), for example a recently claimed detection by Vanzella et al. (2012) also lies in this region. The blue hashed region in the lower left-hand corner shows the range for observed galaxies at $z \approx 0$ which have low values of $f_{esc} \sim 1$ per cent (e.g. Gnedin et al. 2008). The blue circle with error bar represents the Milky Way (Bland-Hawthorn & Maloney 2001), the blue pentagon corresponds to the upper limit in nearby galaxy Haro 11 (Grimes et al. 2007). Most $z \approx 0$ EAGLE galaxies have low values of f_{esc} although unusual outliers exist with high values (blue crosses), comparable to that of the galaxies found by Borthakur et al. (2014, blue star) and Izotov et al. (2016a,b, blue squares with error bars). Many of the $z \approx 3$ galaxies fall in the region of observed LBGs. Finally, a larger number of $z = 6$ galaxies have relatively high values for f_{esc}. The probability distribution for f_{esc} and $\dot{\Sigma}_{\star,0}$ is shown in the panels (b) and (c), respectively, with colours corresponding to the redshift ranges in panel (a).

of 20 per cent allowed by our model. Since $\dot{\Sigma}_\star$ increases with z, galaxies in EAGLE tend to have higher values of f_{esc} at increasing z. At $z = 3$, a considerable fraction has f_{esc} larger than a few per cent, and at $z = 6$ most have $f_{esc} > 10$ per cent.

The low values of f_{esc} at $z \approx 0$ are consistent with those inferred observationally. For example, the Milky Way has an escape fraction of ≈2 per cent (Bland-Hawthorn & Maloney 2001) and Gnedin et al. (2008) find similarly low values for present-day galaxies (with many non-detections). The $z \approx 0$ galaxies discovered by Borthakur et al. (2014) and Izotov et al. (2016a,b) with high escape fractions are clearly exceptional, but such rare exceptions also occur in the simulation where they correspond to vigorously star-forming compact galaxies – just as in the observational data.

Over the past decade or so considerable observational effort has been made to detect ionizing radiation emanating from LBGs at redshifts $z \approx 3$ (e.g. Inoue, Iwata & Deharveng 2006; Shapley et al. 2006; Nestor et al. 2013), yielding mostly non- or controversial detections. Similarly, most EAGLE galaxies at $z = 3$ have very low values of f_{esc} (<1 per cent), with fewer than 10 per cent having $f_{esc} > 10$ per cent that might be detectable observationally, in reasonable agreement with the statistics presented by Siana et al. (2010) and Nestor et al. (2013).

In Fig. 6, we plot the evolution of the UV luminosity-weighted mean escape fraction, $\bar{f}_{esc}$, of the population of EAGLE galaxies, computing the escape fraction for individual star-forming regions as described above (solid red line). The value of $\bar{f}_{esc}$ increases from ≈2 per cent at $z = 0$ to more than 10 per cent above $z = 5$, rising further towards higher z. The trend is well described by $\bar{f}_{esc} \propto (1+z)^{1.1}$ at $z > 3$, with the increase in $\bar{f}_{esc}$ with z much shallower than the $(1+z)^{3.4}$ assumed by Haardt & Madau (2012, black dash–dotted curve in Fig. 6). The figure also shows the evolution that results from combining the dependence of f_{esc} on SFR from individual galaxies from Fig. 5 (black dashed line), with the

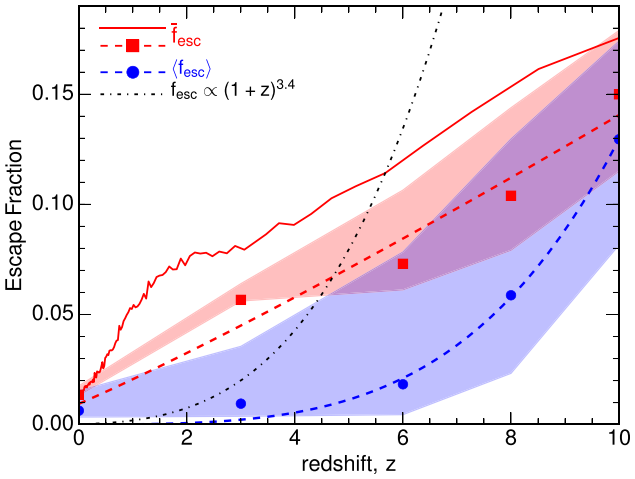

Figure 6. Evolution of the escape fraction of ionizing photons for the population of EAGLE galaxies. The luminosity-weighted mean escape fraction estimated from the model and the simulation, $\bar{f}_{\rm esc}$, is shown as a solid red curve. The evolution of the luminosity-weighted escape fraction computed by using the luminosity-dependent escape fraction at each redshift from the EAGLE simulation, combined with the observed luminosity functions from Bouwens et al. (2015a) integrated down to a faint-end limit of $M_{\rm AB} = -13$ in 1500 Å magnitude, is shown as red squares and fitted with a red dashed curve; the shaded regions show the range where the luminosity functions from Bouwens et al. (2015a) are extrapolated to either -17 to -10. The corresponding results for the galaxy number-weighted escape fraction, $\langle f_{\rm esc} \rangle$, are shown by the blue circles and shaded region; fitted with blue dashed curve. The evolutionary trend from Haardt & Madau (2012) is shown as a black dash–dotted curve, and reaches 100 per cent at $z = 10$. The escape fraction computed with our model evolves with redshift and achieves values $\gtrsim$10 per cent at redshifts $z \gtrsim 5$. The red curve determines the reionization and photoionization history of the Universe, whereas the blue curve is the prediction for the escape fraction for typical observed galaxies at a given redshift.

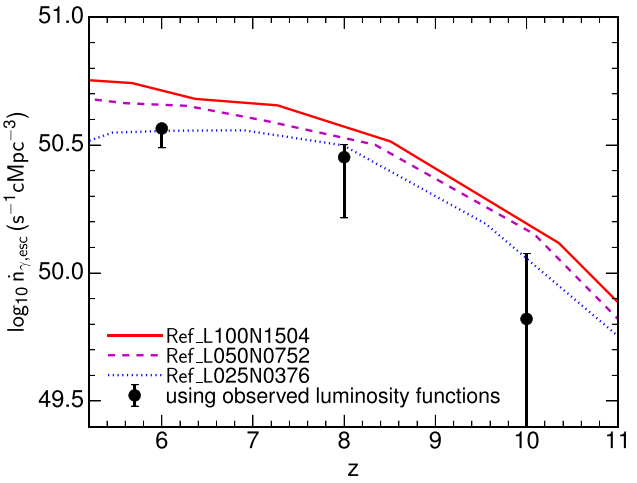

Figure 7. The rate at which ionizing photons escape from galaxies per unit comoving volume, $\dot{n}_{\gamma,\rm esc}$, as a function of redshift using the EAGLE galaxy stellar mass function (dotted blue, dashed magenta and solid red curves correspond to simulations Ref-L025N0376, Ref-L050N0752 and Ref-L100N1504, respectively). Black symbols combine the observed 1500 Å luminosity function extrapolated to $M_{1500,\,\rm AB} = -13$ from Bouwens et al. (2015a) with the evolution of the escape fraction taken from Fig. 5; error bars span the range covered if the faint-end slope is extrapolated to $M_{1500,\,\rm AB} = -10$ and -16.

observed evolution of the luminosity function from Bouwens et al. (2015a), extrapolated to $M_{\rm AB} = -13$ (where $M_{\rm AB}$ is the 1500 Å magnitude on the AB system), either luminosity-weighted ($\bar{f}_{\rm esc}$, red dashed curve) or number-density weighted ($\langle f_{\rm esc} \rangle$, blue curve); the shaded region corresponds to extrapolating to $M_{\rm AB} = -17$ or -10. The luminosity-weighted mean escape fraction can be fitted by $\bar{f}_{\rm esc} = 0.045\,((1+z)/4)^{1.1}$ (red dashed curve) and the number-weighted mean by $\langle f_{\rm esc} \rangle = 2.2 \times 10^{-3}\,((1+z)/4)^4$ at $z > 3$, and the maximum allowed value is 0.2. Since the escape fraction of galaxies in our model is much higher for vigorously star-forming galaxies, we have $\bar{f}_{\rm esc} > \langle f_{\rm esc} \rangle$. However, at higher z, most galaxies are highly star forming and $\bar{f}_{\rm esc} \approx \langle f_{\rm esc} \rangle$. Interestingly, according to the blue curve, most of the LBGs at redshift 3 are predicted to have low ($\lesssim$1 per cent) escape fractions.

Having demonstrated that our model yields the low values of escape fractions observed directly at $z = 0$–3, we proceed to investigate whether $f_{\rm esc}$ at $z \gtrsim 6$ is sufficient to reionize the Universe, and whether the amplitude of the ionizing background, $\Gamma_{\rm H\,I}$, post-reionization is consistent with current observations.

5 APPLICATION TO REIONIZATION

5.1 Emissivity and cumulative photon production

We use the population synthesis model of Schaerer (2003) to calculate the total number of ionizing photons produced by an instantaneous starburst, per unit stellar mass formed, over the lifetime of the stellar population, $\mathrm{d}N_\gamma/\mathrm{d}M_*$, as a function of the initial metallicity. Schaerer (2003) assumes that stars form with a Salpeter stellar IMF (Salpeter 1955) over the stellar mass range 1–100 $\mathrm{M}_\odot$. However, in EAGLE we assume that stars form with a Chabrier (2003) IMF and over a stellar mass range 0.1–100 $\mathrm{M}_\odot$. We therefore divide Schaerer's value of $\mathrm{d}N_\gamma/\mathrm{d}M_*$ by a factor 2.55 to obtain $\mathrm{d}N_\gamma/\mathrm{d}M_*$ for stars forming in the range 0.1–100 $\mathrm{M}_\odot$ and then multiply again by a factor of 1.65 to convert from a Salpeter to a Chabrier IMF. This yields, $\mathrm{d}N_\gamma/\mathrm{d}M_\star \approx 5 \times 10^{60}\,\mathrm{M}_\odot^{-1}$, consistent with the range 2–9 $\times\ 10^{60}\ \mathrm{M}_\odot^{-1}$ found in the study of Topping & Shull (2015), which used a variety of IMFs and included the effect of stellar rotation. This range is probably a good estimate for the uncertainty in this value; the contribution from binary stars is plausibly also important (Stanway et al. 2016).

The total number of ionizing photons escaping galaxies, per unit comoving volume to redshift z, $n_{\gamma,\,\rm esc}$, is then

$$n_{\gamma,\rm esc}(z) = \int_0^\infty f_{\rm esc}(M_\star)\,\frac{\mathrm{d}N_\gamma}{\mathrm{d}M_\star}\,M_\star\,n(M_\star, z)\,\mathrm{d}M_\star, \qquad (4)$$

where $n(M_*, z)$ is the comoving number density of galaxies that formed a total stellar mass, M_*, by redshift z. From this we can compute the emissivity, $\dot{n}_{\gamma,\rm esc}(z) \equiv \mathrm{d}n_{\gamma,\rm esc}/\mathrm{d}t$ – the rate at which ionizing photons escape from galaxies per unit volume at redshift z. We can write this emissivity also as $\dot{n}_{\gamma,\rm esc} \equiv \bar{f}_{\rm esc}\,\dot{n}_{\gamma,\star}$, in terms of the luminosity-weighted mean escape fraction (see Fig. 6) and the rate per comoving volume at which stars produce ionizing photons, $\dot{n}_{\gamma,\star}$.

We calculate $n(M_*, z)$ from our three EAGLE simulations and plot $\dot{n}_{\gamma,\rm esc}$ as a function of redshift in Fig. 7. The emissivity is lower for the simulation of the smallest volume (L025N0376) because it misses the more massive galaxies that contribute significantly to $\dot{n}_\gamma$ in our model. The emissivities for the two larger simulations are within 10 per cent of each other, close enough that errors are

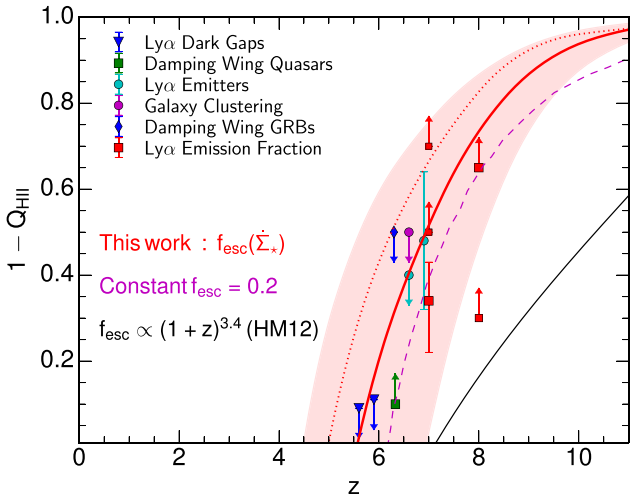

Figure 8. Evolution of the volume filling factor of ionized regions, $Q_{\rm H\,II}$, as a function of redshift. The solid red curve is for the EAGLE simulation and uses our default values for the parameters of the model for the escape fraction, $f_{\rm esc,\,max} = 20$ per cent, $\dot{\Sigma}_{\star,\rm crit} = 0.1\,{\rm M}_\odot\,{\rm yr}^{-1}\,{\rm kpc}^{-2}$. The red shaded region shows the effect of varying $f_{\rm esc,\,max}$ between 10 and 40 per cent. The evolution of $Q_{\rm H\,II}$ found from combining the 1500 Å luminosity function from Bouwens et al. (2015a) with the escape fraction from our model is shown as the red dotted line; the model of Robertson et al. (2015) which assumes $f_{\rm esc} = 20$ per cent for all galaxies is shown as the magenta dashed line; the model of Haardt & Madau (2012) is shown as the black solid line. These models are compared with observed estimates, using Lyα dark gaps statistics (blue triangles; McGreer et al. 2015), the damping wing in a $z = 7$ quasar (green square; Mortlock et al. 2011), the damping wing in gamma-ray burst (black diamond; Totani et al. 2014), galaxy clustering (magenta circle; McQuinn et al. 2007), Lyα emitters (cyan circles; Ota et al. 2008; Ouchi et al. 2010) and the Lyα emission statistics of galaxies (red squares; Caruana et al. 2012; Schenker et al. 2014; Tilvi et al. 2014).

dominated by systematic uncertainties in computing ${\rm d}N_\gamma/{\rm d}M_*$ and $f_{\rm esc}$ rather than $n(M_*, z)$.

The ionizing emissivities computed from the simulation also agree reasonably well with those estimated from observations as $\dot{n}_{\gamma,\rm esc} = \bar{f}_{\rm esc}\, n_{\gamma,\star,\rm obs}$, with $\bar{f}_{\rm esc}$ the fit to the escape fraction from EAGLE found in Section 4, and $n_{\gamma,\star,\rm obs}$ the production rate of ionizing photons calculated by combining the integrated 1500 Å luminosity functions as a function of redshift from Bouwens et al. (2015a), with the conversion factor from Schaerer (2003) between 1500 Å luminosity and ionizing photon luminosity. This agreement is not surprising since EAGLE reproduces the observed luminosity function relatively well, at least up to $z = 6$ (Furlong et al. 2015).

5.2 Timing of reionization

We calculate the evolution of the filling factor of ionized gas, $Q_{\rm H\,II}$, by integrating equation (1) using the results from the EAGLE simulation L0100N1504 for $\dot{n}_{\gamma,\star}$ and $\bar{f}_{\rm esc}$ from Fig 7, and the (extrapolated) evolution of the clumping factor from Pawlik et al. (2009). The result is shown as the red line in Fig. 8 for the default values of the parameters of our model for the escape fraction, $f_{\rm esc,\,max} = 20$ per cent and $\dot{\Sigma}_{\star,\rm crit} = 0.1\,{\rm M}_\odot\,{\rm yr}^{-1}\,{\rm kpc}^{-2}$. The ionized fraction is low at $z = 9$, when $Q_{\rm H\,II} \approx 10$ per cent, reaches 50 per cent by $z = 7$, and 90 per cent by $z = 6$. This evolution is very similar to that obtained from combining the observed 1500 Å luminosity function extrapolated to $M_{1500,\,\rm AB} = -13$ from Bouwens et al. (2015a) with our inferred evolution of $\bar{f}_{\rm esc}$ (dotted red curve) and also to that of the model from Robertson et al. (2015) who take $f_{\rm esc} = 20$ per cent for all galaxies (green curve). The transition from mostly neutral to mostly ionized is much faster in all these models than in the model of Haardt & Madau (2012, solid black line). The red shaded region illustrates the dependence of our model on the value of $f_{\rm esc,\,max}$, showing the range obtained if the value is varied between 10 and 40 per cent.

Inferred values for $Q_{\rm H\,II}(z)$ from observations are based on a variety of methods that are all relatively indirect. Measurements based on the statics of gaps with non-zero transmission in the Lyα region of quasars (e.g. McGreer et al. 2015), on the damping wing observed in a quasar spectrum (Mortlock et al. 2011) or a gamma-ray burst spectrum (Totani et al. 2014) and on the Lyα emission properties of high-z galaxies (e.g Caruana et al. 2012; Schenker et al. 2014; Tilvi et al. 2014) all suggest a relatively rapid increase in $Q_{\rm H\,II}(z)$ from $z = 8$ to 6 (see also Bouwens et al. 2015b; Robertson et al. 2015). These values are uncertain, but they fit very well with the relatively rapid evolution inferred from EAGLE. Becker et al. (2015) report the detection of an extremely long and dark Lyα trough extending down to $z = 5.5$, which they argue is consistent with variations in the mean free path expected to occur near the end of reionization. This interpretation is consistent with the evolution of $Q_{\rm H\,II}(z)$ inferred from both the data and the EAGLE model in Fig. 8.

5.3 Thomson optical depth

The optical depth due to Thomson scattering of cosmic microwave background (CMB) photons of free electrons, $\tau_{\rm es}(z)$, is a measure of the total column density of free electrons between $z = 0$ and a given redshift, and has been measured from the *Planck* satellite data (Planck Collaboration XLVII 2016) for $z = z_{\rm CMB} \approx 1100$, the redshift of the last scattering surface. Within our model for reionization, it can be calculated from the evolution of the ionized fraction $Q_{\rm H\,II}(z)$ as

$$\tau_{\rm es}(z) = \int_0^z 1.08\,\sigma_{\rm T}\, Q_{\rm H\,II}(z)\, n_{\rm H}(z)\; c\, H(z)^{-1}\, {\rm d}z, \qquad (5)$$

where $\sigma_{\rm T}$ is the Thomson cross-section, and the factor 1.08 takes into account singly ionized helium. We plot $\tau_{\rm es}(z)$ for our default model of reionization with $f_{\rm esc,\,max} = 20$ per cent as the red curve in Fig. 9, as well as a model based on the observed 1500 Å luminosity function extrapolated to $M_{1500,\,\rm AB} = -13$ from Bouwens et al. (2015a) with our inferred evolution of $\bar{f}_{\rm esc}$ (solid red line) and the model from Robertson et al. (2015) which assumes $f_{\rm esc} = 20$ per cent (magenta line). These all yield very similar results and all fall well below the model of Haardt & Madau (2012, solid black line). The models are compared to the constraints from *Planck* (Planck Collaboration XLVII 2016) which apply to $z = z_{\rm CMB}$ only, shown as the blue shaded region.[5] The EAGLE model is consistent with the *Planck* constraints. The effects of varying $f_{\rm esc,\,max}$ between 10 and 40 per cent are illustrated by the red shaded region.

5.4 The amplitude of the UV-background post-reionization

Models for the evolution of the escape fraction should also reproduce the observed photoionization rate, $\Gamma_{\rm H\,I}$, after reionization. The

[5] The 2016 *Planck* value of the optical depth is ∼20 per cent lower than the 2015 value and is in much better agreement with our model predictions.

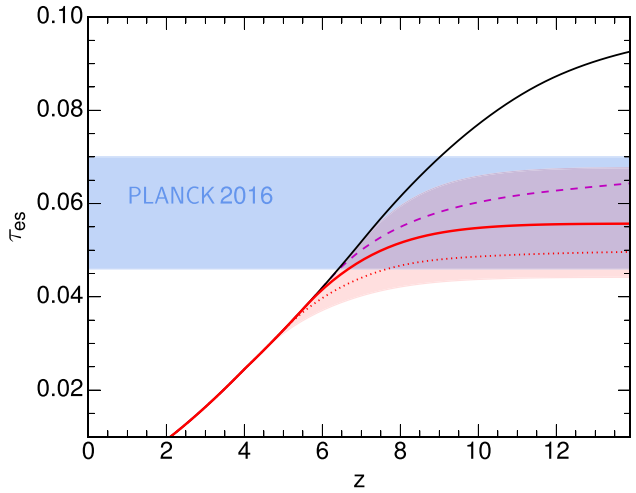

Figure 9. As Fig. 8 but for the Thomson scattering optical depth, τ_{es}, as a function of redshift. As before, the solid red line is for EAGLE galaxies using our default parameters for the evolution of the escape fraction. The horizontal shaded blue region demarcates the allowed 1σ range from recent *Planck* results (Planck Collaboration XLVII 2016); the EAGLE model is in good agreement with these data, as is the model of Robertson et al. (2015), shown as the magenta dashed line, which assumes $f_{esc} = 20$ per cent for all galaxies, By contrast, the model by Haardt & Madau (2012, black solid line) overestimates τ_{es}.

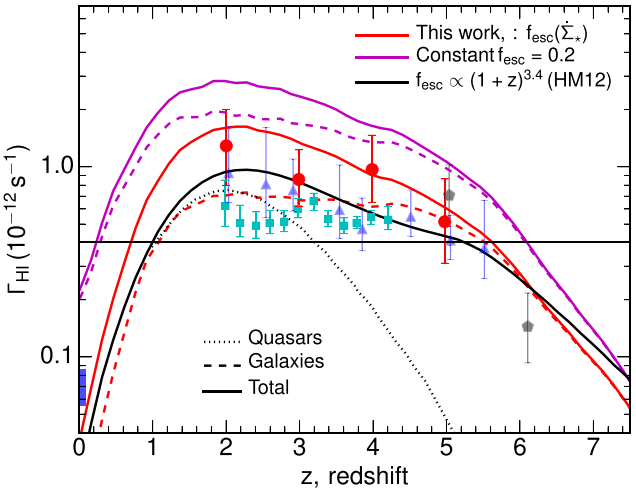

Figure 10. The H I photoionization rate, $\Gamma_{H\,I}$, as a function of redshift. The dotted black curve is the contribution from quasars taken from Haardt & Madau (2012), the dashed red line is the contribution from EAGLE galaxies using the escape fraction from this paper and the red line is the sum of both. The photoionization rate from Haardt & Madau (2012) is shown as the black line, and a model based on EAGLE but using a constant value of $f_{esc} = 20$ per cent is shown with magenta lines (dashed: galaxies only; full line: including QSOs). Various measurements based on the effective opacity in the Lyα forest are shown for comparison: red circles (Bolton & Haehnelt 2007); blue triangles (Becker, Rauch & Sargent 2007); cyan squares (Faucher-Giguère et al. 2008); measurements from the quasar near zones shown as grey pentagons (Calverley et al. 2011); measurement at $z \approx 0$ shown as blue vertical bar (Fumagalli et al. 2017).

photoionization rate is inferred observationally from measuring the mean transmission in the Lyα forest of high-z quasi-stellar objects (QSOs), but that quantity is degenerate with the poorly constrained temperature of the IGM and the level of small-scale clustering of gas (e.g. Rauch et al. 1997). The photoionization rate is related to the ionizing emissivity through the mean free path of ionizing photons, which is closely related to the mean distance between LLSs. We use the method that relates emissivity and photoionization rate developed by Haardt & Madau (2012) to compute $\Gamma_{H\,I}$ from EAGLE galaxies. Adding the contribution from QSOs computed by those authors, we compare the net rate to other model predictions as well as observations in Fig. 10.

The value of $\Gamma_{H\,I}$ obtained by combining the contribution of EAGLE galaxies with that of QSOs rises by a factor of 10 between $z = 8$ and 4, remains constant to within a factor of 2 to $z = 1.5$, and then drops rapidly towards $z = 0$. The contribution of galaxies dominates above $z = 2$, is close to 90 per cent of the total at $z = 4$ and increases even further towards higher z. Our values are higher than those of Haardt & Madau (2012) because of the shallower evolution of the escape fraction in our case. Our calculations of f_{esc} do not consider absorption by dust, which should play an increasingly important role at lower z. We may therefore increasingly overestimate $\Gamma_{H\,I}$ towards lower z.

Bolton & Haehnelt (2007) and Becker et al. (2007) quote uncertainties in the measured values of $\Gamma_{H\,I}$ of 50 per cent or more but, in addition, there appear to be systematic differences in their values compared to those of Faucher-Giguère et al. (2008). The values we infer from EAGLE at $z = 2$–3 agree very well with the data of Bolton & Haehnelt (2007) and are slightly higher than the data of Becker et al. (2007) and, at best, are marginally consistent with the data of Faucher-Giguère et al. (2008) which have the smallest error bars. The agreement with these data sets improves at higher z, but our model predictions are somewhat above the value inferred by Calverley et al. (2011) from the quasar near zone measurement at $z \approx 6$.

A model in which $f_{esc} = 20$ per cent (magenta line), similar to that discussed by Robertson et al. (2015) and Bouwens et al. (2015b), yields similar values of $\Gamma_{H\,I}$ to those from our EAGLE model (red curve) down to $z \approx 7$, but yields values that become increasingly high at lower redshifts. At $z = 0$ such a model predicts $\Gamma_{H\,I}(z = 0) \approx 2 \times 10^{-13}$ s^{-1}, more than an order of magnitude above the $z = 0$ upper limit of Adams et al. (2011) (see also Fumagalli et al. 2017). This demonstrates once again that the escape fraction *has* to vary with z, in order to reconcile the low values of $\Gamma_{H\,I}$ measured below $z = 1$, say, with the relatively high values inferred above $z = 5$ (see also Khaire et al. 2016). However the evolution cannot be as steep as that proposed by Haardt & Madau (2012), $f_{esc} \propto (1+z)^{3.4}$, because that conflicts with the evolution of $Q_{H\,II}$ and the measured $\tau_{es}(z = z_{CMB})$ discussed above.

The photoionization rate due to quasars alone from Haardt & Madau (2001), shown as a dotted line in Fig. 10, decreases rapidly with increasing redshift above $z \sim 2$ due to the steep decline in the number density of (relatively) bright quasars. In a recent study, Giallongo et al. (2015) suggest that the number density of faint quasars decreases much less rapidly beyond $z = 3$. Madau & Haardt (2015) extrapolate the data presented by Giallongo et al. (2015) and claim that such faint quasars by themselves emit enough ionizing photons to ionize the Universe (see also Mitra, Choudhury & Ferrara 2016). However, adding the contribution that results from this extrapolation, taken from fig. 3 in Madau & Haardt (2015), would double the value of $\Gamma_{H\,I}$ at $z = 5$, and almost triple it at $z = 6$. Such high values may be in tension with observations, especially at $z = 6$. Future observations should clarify the contribution of quasars to $\Gamma_{H\,I}$ and to reionization.

6 SUMMARY

The fraction of ionizing photons that escapes from galaxies are not well constrained observationally and theoretical predictions vary widely. The low values of the escape fraction measured locally and the strong indication that the Universe reionized close to redshifts $z = 6$–8 requires $f_{\rm esc}$ to evolve strongly with z, increasing from a few per cent at $z = 0$ to ∼20 per cent above $z = 6$. Here we presented a model based on the EAGLE simulations that explains this evolution.

In the EAGLE simulations, the median density at which stars form increases rapidly with redshift. This implies that stars form at increasingly higher pressure, or equivalently, star formation surface density, $\dot{\Sigma}_\star$, and yields smaller galaxies with higher sSFRs with increasing z. Physically this is a consequence of the larger cosmological accretion rate on to galaxies at higher z, combined with the evolution of the efficiency of feedback from star formation. Such a trend is also seen observationally since galaxy sSFRs increase rapidly with z whereas galaxy sizes decrease. Indeed, in Sharma et al. (2016) we showed that EAGLE reproduces the observed evolution of star formation surface densities.

Star formation at high values of $\dot{\Sigma}_\star$ is observed to result in strong galactic winds (e.g. Heckman et al. 2011), and indeed, such winds, although rare at $z = 0$, are ubiquitous at higher z (e.g. Pettini et al. 2002; Weiner et al. 2009; Bradshaw et al. 2013). Following Sharma et al. (2016), we assumed that winds increase the fraction of ionizing photons that can escape their galaxy through channels carved by outflows through the neutral gas in the ISM. Our model has two main parameters: $\dot{\Sigma}_{\star,\rm crit}$, the SFR surface density above which strong winds are launched, and $f_{\rm esc,max}$, the escape fraction in the presence of such winds. Therefore, the escape fraction is large in compact starbursts; there is some observational evidence supporting this (Borthakur et al. 2014; de Barros et al. 2016; Izotov et al. 2016a,b). As in Sharma et al. (2016) we use $\dot{\Sigma}_{\star,\rm crit} = 0.1\,{\rm M}_\odot\,{\rm yr}^{-1}\,{\rm kpc}^{-2}$, as suggested by Heckman (2001), and $f_{\rm esc,\,max} = 20$ per cent, motivated by the observations of Borthakur et al. (2014) of the escape fraction in a $z \sim 0$ compact starburst.

Applying this model to star formation in EAGLE we find that $f_{\rm esc}$ increases rapidly with redshift, from very low values at $z = 0$ to nearly 20 per cent at $z > 6$. This occurs because very few galaxies form stars with $\dot{\Sigma}_\star \geq \dot{\Sigma}_{\star,\rm crit}$ at low z, whereas most do so at $z > 6$ (Fig. 2). As a consequence, $f_{\rm esc}$ evolves rapidly enough to yield a realistic evolution for the filling factor of ionized gas (Fig. 8), the Thomson optical depth to the surface of last scattering (Fig. 9) and the amplitude of the ionizing background post-reionization (Fig. 10). In particular, we find the following.

(i) The escape fraction depends strongly on the central surface density of star formation, $\dot{\Sigma}_{\star,0}$, approximately as $f_{\rm esc} = 0.2/(1 + \dot{\Sigma}_{\star,\rm crit}/\dot{\Sigma}_{\star,0})$ (Fig. 5).

(ii) The luminosity-weighted mean escape fraction in the absence of dust, averaged over the galaxy population, evolves as $\bar{f}_{\rm esc} = 0.045\,((1+z)/4)^{1.1}$ and becomes constant at ≈0.2 at redshift $z > 10$. The galaxy number-weighted mean escape fraction of galaxies as a function of redshift evolves as $f_{\rm esc} = 2.2 \times 10^{-3}\,((1+z)/4)^4$, and becomes constant once it attains a maximum value of 0.2 at high redshift (Fig. 6).

(iii) The escape fraction is, in general, higher for brighter star-forming galaxies at a given stellar mass (Fig. 4). As a consequence faint galaxies below the *HST* Ultra Deep Field (UDF) detection limit do not dominate the photon budget for reionization (Sharma et al. 2016).

A complete theoretical understanding of the physics governing the dependence of the escape fraction on $\dot{\Sigma}_\star$ is lacking. It would require accurate radiation-hydrodynamic modelling of the ISM and of individual star-forming regions, including the radiative and energetic feedback from massive stars and SNe. Recent studies have achieved some progress towards this goal by concentrating on small galaxies at high z (e.g. Wise & Cen 2009; Kimm & Cen 2014; Ma et al. 2015), although even these lack the resolution and physics required to capture the intricacies that influence the escape fraction at the scale of molecular clouds.

In the case where massive stars carve the channels through which photons can escape, there may still be a timing issue preventing a galaxy from having a high emissivity. Indeed, the production of ionizing photons may have decreased significantly already before the channels are opened, given the short lifetime of massive stars. The emissivity may then be low when the escape fraction is high. Ionizing photons emitted by binary stars (Stanway et al. 2016) may help overcome this (see also Ma et al. 2016).

We have neglected the effects of dust, except in the calculation of $\Gamma_{\rm H\,I}$. Dust likely has a negligible effect at high z ($z > 6$, say), given that observed sources at high redshift are dust poor (Bouwens et al. 2015a). Dust may, however, play a much more important role at lower redshifts, potentially explaining the fact that many low-redshift detections report low values of $f_{\rm esc}$ despite the highly eruptive nature of many of the galaxies investigated (Leitet et al. 2013). The escape fraction reported by Borthakur et al. (2014) is reduced from 20 to ≈2 per cent if the effect of dust is taken into account.

Reionization in our model proceeds quite rapidly, much faster than in the model of Haardt & Madau (2012), as illustrated in Fig. 8. One reason for this is that the escape fraction in the simulations declines more slowly with decreasing redshift than in the Haardt & Madau (2012) model, giving rise to a steeper build-up of the emissivity. The rate of evolution of the emissivity (and thus the speed at which reionization occurs) depends, of course, on the rate of evolution of the galaxy luminosity function. Both in our simulations and in the data, the bright end of the luminosity function evolves faster than the faint end (e.g. Bouwens et al. 2015a). Since the production of ionizing photons in our model is dominated by brighter galaxies (Sharma et al. 2016), the emissivity and the volume filling factor, $Q_{\rm H\,II}$, evolve quite rapidly.

Here we find that the brighter galaxies dominate reionization (see also Sharma et al. 2016), in apparent contradiction with studies that claim that *faint* galaxies are the drivers of reionization (e.g. Yajima et al. 2011; Wise et al. 2014). In the model by Wise et al. (2014), galaxies that contribute to reionization have $M_{1500} \sim -17$ (their fig. 15) and are hosted by haloes of mass $M_{\rm h} \approx 10^8\,{\rm M}_\odot$ (their fig. 8) at $z = 7$. These values, in fact, agree well with our findings (see Fig. 4). We also agree that lower mass galaxies with lower SFRs contribute progressively more with increasing z. The reason for the difference in interpretation, notwithstanding the similarity in results, is twofold. (i) Reionization is relatively rapid in our model, with the volume filling factor of ionized gas increasing from $Q_{\rm H\,II} = 0.2$ at $z = 8$ to $Q_{\rm H\,II} = 0.8$ at $z = 6$. In fact, half of all ionizations occurring below $z = 7$, galaxies that dominate the ionizing emissivity at $z \gtrsim 8$ are therefore not particularly relevant for *reionization* itself. (ii) We call the $z \sim 7$ galaxies brighter than $M_{1500} = -17$ bright because they are comfortably above the *HST* detection limit. It is in this sense that we claim that the brighter galaxies reionized the Universe: our model does not need to appeal to a putative population of galaxies much fainter than current (or future) detection limits, for galaxies to be able to reionize the Universe.

Existing observational data, displayed in Fig. 8, support the steep history of reionization as obtained in this work. (Radiative transfer calculations suggest that reionization might have slowed down near the end due to the effect of LLSs; e.g. Shukla et al. 2016.) Future observational surveys should constrain the evolution of the ionized fraction better and thus shed light on the nature of the sources that reionized the Universe.

An ab initio calculation of the escape fraction remains an important, if challenging, goal of theoretical studies of reionization. Our model, in which the escape of photons is determined by the ability of galaxies to drive winds, exhibits the right phenomenology to explain why $f_{\rm esc}$ evolves rapidly with z and may help guide such studies. From an observational perspective, the inference of $f_{\rm esc}$ from the detection of nebular emission lines in early star-forming galaxies with *James Webb Space Telescope* (*JWST*; e.g. Erb et al. 2016) will provide an important test of our model.

ACKNOWLEDGEMENTS

We are grateful to Lydia Heck and Peter Draper for supporting with their expertise in high performance computing. We thank PRACE for the access to the Curie facility in France. We have used the DiRAC system which is a part of National E-Infrastructure at Durham University, operated by the Institute for Computational Cosmology on behalf of the STFC DiRAC HPC Facility (www.dirac.ac.uk); the equipment was funded by BIS National E-infrastructure capital grant ST/K00042X/1, STFC capital grant ST/H008519/1, STFC DiRAC Operations grant ST/K003267/1 and Durham University. The study was sponsored by the Dutch National Computing Facilities Foundation (NCF) for the use of supercomputer facilities, with financial support from the Netherlands Organisation for Scientific Research (NWO), and the European Research Council under the European Union's Seventh Framework Programme (FP7/2007- 2013)/ERC Grant agreements 278594 GasAroundGalaxies, GA 267291 Cosmiway and 321334 DUSTYGAL. Support was also received via the Interuniversity Attraction Poles Programme initiated by the Belgian Science Policy Office ([AP P7/08 CHARM]), the National Science Foundation under Grant No. NSF PHY11-25915 and the UK Science and Technology Facilities Council (grant numbers ST/F001166/1 and ST/I000976/1) via rolling and consolidating grants awarded to the ICC. RAC is a Royal Society university research fellow. MSh is an STFC Postdoctoral fellow at the ICC. Some of the data in this paper are available in the EAGLE data base, available on request to McAlpine et al. (2016) or to the authors.

REFERENCES

Abel T., Haehnelt M. G., 1999, ApJ, 520, L13
Adams J. J., Uson J. M., Hill G. J., MacQueen P. J., 2011, ApJ, 728, 107
Altay G., Theuns T., Schaye J., Booth C. M., Dalla Vecchia C., 2013, MNRAS, 436, 2689
Barkana R., Loeb A., 2001, Phys. Rep., 349, 125
Becker G. D., Rauch M., Sargent W. L. W., 2007, ApJ, 662, 72
Becker G. D., Bolton J. S., Madau P., Pettini M., Ryan-Weber E. V., Venemans B. P., 2015, MNRAS, 447, 3402
Bland-Hawthorn J., Maloney P. R., 2001, ApJ, 550, L231
Bolton J. S., Haehnelt M. G., 2007, MNRAS, 382, 325
Booth C. M., Schaye J., 2009, MNRAS, 398, 53
Booth C. M., Schaye J., Delgado J. D., Dalla Vecchia C., 2012, MNRAS, 420, 1053
Borthakur S., Heckman T. M., Leitherer C., Overzier R. A., 2014, Science, 346, 216
Bouwens R. J. et al., 2015a, ApJ, 803, 34
Bouwens R. J., Illingworth G. D., Oesch P. A., Caruana J., Holwerda B., Smit R., Wilkins S., 2015b, ApJ, 811, 140
Bradshaw E. J. et al., 2013, MNRAS, 433, 194
Bridge C. R. et al., 2010, ApJ, 720, 465
Calverley A. P., Becker G. D., Haehnelt M. G., Bolton J. S., 2011, MNRAS, 412, 2543
Caruana J., Bunker A. J., Wilkins S. M., Stanway E. R., Lacy M., Jarvis M. J., Lorenzoni S., Hickey S., 2012, MNRAS, 427, 3055
Chabrier G., 2003, PASP, 115, 763
Chevalier R. A., Gardner J., 1974, ApJ, 192, 457
Ciardi B., Ferrara A., Governato F., Jenkins A., 2000, MNRAS, 314, 611
Clarke C., Oey M. S., 2002, MNRAS, 337, 1299
Crain R. A. et al., 2015, MNRAS, 450, 1937
Daddi E. et al., 2007, ApJ, 670, 156
Dalla Vecchia C., Schaye J., 2012, MNRAS, 426, 140
Damen M., Labbé I., Franx M., van Dokkum P. G., Taylor E. N., Gawiser E. J., 2009, ApJ, 690, 937
de Barros S. et al., 2016, A&A, 585, A51
Erb D. K., Quider A. M., Henry A. L., Martin C. L., 2012, ApJ, 759, 26
Erb D. K., Pettini M., Steidel C. C., Strom A. L., Rudie G. C., Trainor R. F., Shapley A. E., Reddy N. A., 2016, ApJ, 830, 52
Faisst A. L., 2016, ApJ, 829, 99
Fan X., Carilli C. L., Keating B., 2006, ARA&A, 44, 415
Faucher-Giguère C.-A., Lidz A., Hernquist L., Zaldarriaga M., 2008, ApJ, 682, L9
Freundlich J. et al., 2013, A&A, 553, A130
Fujita A., Martin C. L., Mac Low M.-M., Abel T., 2003, ApJ, 599, 50
Fumagalli M., Haardt F., Theuns T., Morris S. L., Cantalupo S., Madau P., Fossati M., 2017, MNRAS, preprint (arXiv:1702.04726)
Furlanetto S. R., Oh S. P., 2016, MNRAS, 457, 1813
Furlong M. et al., 2015, MNRAS, 450, 4486
Furlong M. et al., 2017, MNRAS, 465, 722
Gentry E. S., Krumholz M. R., Dekel A., Madau P., 2017, MNRAS, 465, 2471
Genzel R. et al., 2011, ApJ, 733, 101
Giallongo E. et al., 2015, A&A, 578, A83
Gnedin N. Y., 2000, ApJ, 535, 530
Gnedin N. Y., 2016, ApJ, 825, L17
Gnedin N. Y., Kravtsov A. V., Chen H.-W., 2008, ApJ, 672, 765
González V., Bouwens R., Illingworth G., Labbé I., Oesch P., Franx M., Magee D., 2014, ApJ, 781, 34
Grimes J. P. et al., 2007, ApJ, 668, 891
Haardt F., Madau P., 2001, in Neumann D. M., Tran J. T. V., eds, Clusters of Galaxies and the High Redshift Universe Observed in X-rays. CEA, Saclay, p. 64
Haardt F., Madau P., 2012, ApJ, 746, 125
Haas M. R., Schaye J., Booth C. M., Dalla Vecchia C., Springel V., Theuns T., Wiersma R. P. C., 2013, MNRAS, 435, 2931
Heckman T. M., 2001, in Hibbard J. E., Rupen M., van Gorkom J. H., eds, ASP Conf. Ser. Vol. 240, Gas and Galaxy Evolution. Astron. Soc. Pac., San Francisco, p. 345
Heckman T. M., 2002, in Mulchaey J. S., Stocke J. T., eds, ASP Conf. Ser. Vol. 254, Extragalactic Gas at Low Redshift. Astron. Soc. Pac., San Francisco, p. 292
Heckman T. M. et al., 2011, ApJ, 730, 5
Iliev I., Santos M., Mesinger A., Majumdar S., Mellema G., 2015, Proceedings of Advancing Astrophysics with the Square Kilometre Array (AASKA14). Online at http://pos.sissa.it/cgi-bin/reader/conf.cgi?confid=215, id.7
Inoue A. K., Iwata I., Deharveng J.-M., 2006, MNRAS, 371, L1
Iwata I. et al., 2009, ApJ, 692, 1287
Izotov Y. I., Orlitová I., Schaerer D., Thuan T. X., Verhamme A., Guseva N. G., Worseck G., 2016a, Nature, 529, 178
Izotov Y. I., Schaerer D., Thuan T. X., Worseck G., Orlitova I., Verhamme A., 2016b, MNRAS, 461, 3683
Jenkins A., 2013, MNRAS, 434, 2094

Kawamata R., Ishigaki M., Shimasaku K., Oguri M., Ouchi M., 2015, ApJ, 804, 103
Keller S. C. et al., 2014, Nature, 506, 463
Kennicutt R. C. Jr., 1998, ARA&A, 36, 189
Kennicutt R. C. Jr., et al., 2003, PASP, 115, 928
Khaire V., Srianand R., Choudhury T. R., Gaikwad P., 2016, MNRAS, 457, 4051
Kimm T., Cen R., 2014, ApJ, 788, 121
Leitet E., Bergvall N., Hayes M., Linné S., Zackrisson E., 2013, A&A, 553, A106
Ma X., Kasen D., Hopkins P. F., Faucher-Giguère C.-A., Quataert E., Kereš D., Murray N., 2015, MNRAS, 453, 960
Ma X., Hopkins P. F., Kasen D., Quataert E., Faucher-Giguere C.-A., Keres D., Murray N., 2016, MNRAS, 459, 3614
McAlpine S. et al., 2016, Astron. Comput., 15, 72
McGreer I. D., Mesinger A., D'Odorico V., 2015, MNRAS, 447, 499
McQuinn M., Hernquist L., Zaldarriaga M., Dutta S., 2007, MNRAS, 381, 75
Madau P., Haardt F., 2015, ApJ, 813, L8
Madau P., Ferrara A., Rees M. J., 2001, ApJ, 555, 92
Mather J. C. et al., 1994, ApJ, 420, 439
Matthee J., Sobral D., Best P., Khostovan A. A., Oteo I., Bouwens R., Röttgering H., 2017, MNRAS, 465, 3637
Mellema G. et al., 2013, Exp. Astron., 36, 235
Miralda-Escudé J., Haehnelt M., Rees M. J., 2000, ApJ, 530, 1
Mitchell P. D., Lacey C. G., Baugh C. M., Cole S., 2013, MNRAS, 435, 87
Mitra S., Choudhury T. R., Ferrara A., 2015, MNRAS, 454, L76
Mitra S., Choudhury T. R., Ferrara A., 2016, preprint (arXiv:1606.02719)
Mortlock D. J. et al., 2011, Nature, 474, 616
Mostardi R. E., Shapley A. E., Steidel C. C., Trainor R. F., Reddy N. A., Siana B., 2015, ApJ, 810, 107
Murray N., Ménard B., Thompson T. A., 2011, ApJ, 735, 66
Nestor D. B., Shapley A. E., Kornei K. A., Steidel C. C., Siana B., 2013, ApJ, 765, 47
Noeske K. G. et al., 2007, ApJ, 660, L47
Ono Y. et al., 2012, ApJ, 744, 83
Ota K. et al., 2008, ApJ, 677, 12
Ouchi M. et al., 2010, ApJ, 723, 869
Paardekooper J.-P., Khochfar S., Dalla Vecchia C., 2015, MNRAS, 451, 2544
Pawlik A. H., Schaye J., van Scherpenzeel E., 2009, MNRAS, 394, 1812
Pawlik A. H., Schaye J., Dalla Vecchia C., 2015, MNRAS, 451, 1586
Pawlik A. H., Rahmati A., Schaye J., Jeon M., Dalla Vecchia C., 2017, MNRAS, 466, 960
Pettini M., Shapley A. E., Steidel C. C., Cuby J.-G., Dickinson M., Moorwood A. F. M., Adelberger K. L., Giavalisco M., 2001, ApJ, 554, 981
Pettini M., Rix S. A., Steidel C. C., Adelberger K. L., Hunt M. P., Shapley A. E., 2002, ApJ, 569, 742
Planck Collaboration XVI, 2014, A&A, 571, A16
Planck Collaboration XLVII, 2016, A&A, 596, A108
Price L. C., Trac H., Cen R., 2016, preprint (arXiv:1605.03970)
Rauch M. et al., 1997, ApJ, 489, 7
Razoumov A. O., Sommer-Larsen J., 2006, ApJ, 651, L89
Razoumov A. O., Sommer-Larsen J., 2010, ApJ, 710, 1239
Reddy N. A., Steidel C. C., 2009, ApJ, 692, 778
Robertson B. E., Ellis R. S., Furlanetto S. R., Dunlop J. S., 2015, ApJ, 802, L19
Rosas-Guevara Y. M. et al., 2015, MNRAS, 454, 1038
Rutkowski M. J. et al., 2016, ApJ, 819, 81
Salpeter E. E., 1955, ApJ, 121, 161
Scannapieco E., 2013, ApJ, 763, L31
Scannapieco E., Gray W. J., Pan L., 2012, ApJ, 746, 57
Schaerer D., 2003, A&A, 397, 527
Schaller M., Dalla Vecchia C., Schaye J., Bower R. G., Theuns T., Crain R. A., Furlong M., McCarthy I. G., 2015, MNRAS, 454, 2277
Schaye J., 2004, ApJ, 609, 667
Schaye J., Dalla Vecchia C., 2008, MNRAS, 383, 1210
Schaye J. et al., 2010, MNRAS, 402, 1536
Schaye J. et al., 2015, MNRAS, 446, 521
Schenker M. A., Ellis R. S., Konidaris N. P., Stark D. P., 2014, ApJ, 795, 20
Shapley A. E., Steidel C. C., Pettini M., Adelberger K. L., 2003, ApJ, 588, 65
Shapley A. E., Steidel C. C., Pettini M., Adelberger K. L., Erb D. K., 2006, ApJ, 651, 688
Sharma M., Theuns T., Frenk C., Bower R., Crain R., Schaller M., Schaye J., 2016, MNRAS, 458, L94
Shibuya T., Ouchi M., Harikane Y., 2015, ApJS, 219, 15
Shirazi M., Brinchmann J., Rahmati A., 2014, ApJ, 787, 120
Shukla H., Mellema G., Iliev I. T., Shapiro P. R., 2016, MNRAS, 458, 135
Siana B. et al., 2007, ApJ, 668, 62
Siana B. et al., 2010, ApJ, 723, 241
Springel V., 2005, MNRAS, 364, 1105
Springel V., Di Matteo T., Hernquist L., 2005, MNRAS, 361, 776
Stanway E. R., Eldridge J. J., Becker G. D., 2016, MNRAS, 456, 485
Stark D. P., Schenker M. A., Ellis R., Robertson B., McLure R., Dunlop J., 2013, ApJ, 763, 129
Stiavelli M. et al., 2009, Astro2010: The Astronomy and Astrophysics Decadal Survey, Science White Papers, no. 287
Strickland D. K., Heckman T. M., 2009, ApJ, 697, 2030
Swinbank A. M., Smail I., Sobral D., Theuns T., Best P. N., Geach J. E., 2012, ApJ, 760, 130
Theuns T., Viel M., Kay S., Schaye J., Carswell R. F., Tzanavaris P., 2002, ApJ, 578, L5
Tilvi V. et al., 2014, ApJ, 794, 5
Topping M. W., Shull J. M., 2015, ApJ, 800, 97
Totani T. et al., 2014, PASJ, 66, 63
Trainor R. F., Steidel C. C., Strom A. L., Rudie G. C., 2015, ApJ, 809, 89
Trayford J. W. et al., 2015, MNRAS, 452, 2879
Trayford J. W., Theuns T., Bower R. G., Crain R. A., Lagos C. d. P., Schaller M., Schaye J., 2016, MNRAS, 460, 3925
Vanzella E. et al., 2012, ApJ, 751, 70
von Glasow W., Krause M. G. H., Sommer-Larsen J., Burkert A., 2013, MNRAS, 434, 1151
Weiner B. J. et al., 2009, ApJ, 692, 187
White S. D. M., Frenk C. S., 1991, ApJ, 379, 52
White S. D. M., Rees M. J., 1978, MNRAS, 183, 341
Wiersma R. P. C., Schaye J., Smith B. D., 2009a, MNRAS, 393, 99
Wiersma R. P. C., Schaye J., Theuns T., Dalla Vecchia C., Tornatore L., 2009b, MNRAS, 399, 574
Wise J. H., Cen R., 2009, ApJ, 693, 984
Wise J. H., Demchenko V. G., Halicek M. T., Norman M. L., Turk M. J., Abel T., Smith B. D., 2014, MNRAS, 442, 2560
Xu H., Wise J. H., Norman M. L., Ahn K., O'Shea B. W., 2016, ApJ, 833, 84
Yajima H., Choi J.-H., Nagamine K., 2011, MNRAS, 412, 411
Zastrow J., Oey M. S., Veilleux S., McDonald M., Martin C. L., 2011, ApJ, 741, L17
Zastrow J., Oey M. S., Veilleux S., McDonald M., 2013, ApJ, 779, 76

This paper has been typeset from a TEX/LATEX file prepared by the author.